

CLIMATE IMPACT AND ECONOMIC ASSESSMENT OF LIQUID HYDROGEN AND SYNTHETIC KEROSENE LONG-RANGE AIRCRAFT CONCEPTS

Sebastian Wöhler¹, Kuno Buchtal², Michael Iwanizki³, Jannik Häßy⁴, Katrin Dahlmann⁵, Christos Lois² & Martin Hepperle³

¹German Aerospace Center (DLR), Institute of System Architectures in Aeronautics, Hamburg, 21129, Germany
 ²German Aerospace Center (DLR), Institute of Air Transport, Hamburg, 21079, Germany
 ³German Aerospace Center (DLR), Institute of Aerodynamics and Flow Technology, Braunschweig, 38108, Germany
 ⁴German Aerospace Center (DLR), Institute of Propulsion Technology, Köln, 51147, Germany
 ⁵German Aerospace Center (DLR), Institute of Atmospheric Physics, Oberpfaffenhofen-Wessling, 82234, Germany

Abstract

Economic efficiency, energy demand and environmental impact are the key design drivers for the next major change in aviation towards a sustainable aviation industry. For the long range market segment, alternative energy carriers are essential to meet the goals of the European Green Deal, as battery electric flight or hybrid propulsion system architectures are not suitable at the current state of the art. Therefore, this paper covers the economic and climate impact assessment of fossil kerosene, sustainable aviation fuel and liquid hydrogen as energy sources for the long range market segment of a potential next generation aircraft assuming a technology scenario expected to be ready in 2035.

To explore additional potential of climate impact reduction mainly related to the contrail induced cloudiness and NOx emissions, variations of flight altitudes and design Mach numbers are carried out. These studies are conducted for the three types of fuels with aircraft designed for each specific parameter combination. The impact of those design changes on the average temperature response and the direct operating costs are finally evaluated.

Keywords: Climate Impact Assessment, Aircraft Design, Liquid Hydrogen, Sustainable Aviation Fuels, Long Range

1. Motivation

In 2020, almost 95% of the world's flights took place on routes of up to 4,000 km. This implies that only 5% of the world's flights in 2020 will be in the long-haul segment beyond 4,000 km. However, despite their small number, long-haul flights are responsible for 40% of aviation's CO2 emissions. The long-haul segment therefore has the second largest climate impact of aviation, second only to the short- and medium-haul segment, at 51% [1]. This is mainly due to the significantly greater range of up to 16,700 km (non-stop scheduled flight from Singapore to New York) and the resulting significantly longer flight time and thus emissions.

Compared to the regional and short-to-medium segments, the ratio of fuel mass to aircraft take-off mass is significantly higher for long-haul aircraft. In the long-haul segment, fuel mass accounts for approximately 40% of take-off mass, compared to 30% in the short-medium segment and less than 20% on average in the regional segment. As a result, aircraft efficiency is more important to the economics of long-haul operations than in other market segments. This has a significant impact on the choice of fuel option to be operated in the long-haul segment. Due to the large design ranges, aircraft efficiency is more important than in other market segments. Batteries and hybrid electric concepts are not suitable for this application due to their low energy density. Therefore, this study focuses on the use of kerosene, sustainable aviation fuel (SAF) and liquid hydrogen (LH2) as primary energy

sources and their direct combustion.

Today's intercontinental fleets of global airlines consist of a wide variety of aircraft models. With the phase-out of very large-capacity aircraft such as the Boeing 747 family and Airbus A380, manufacturers' long-haul product portfolios are currently limited to the Boeing 787 and 777 families and the Airbus A330 and A350, which have passenger capacities ranging from 250 to 400. This study takes this aircraft size as a starting point for designing a successor model for the year 2035.

The study examines the impact of the above-mentioned fuels (kerosene, SAF and LH2) on operating costs and climate impact. In line with the German government's aviation strategy and the European "Flightpath 2050" agenda, the aim is to significantly reduce CO2 emissions and, in particular, the climate impact of CO2 and non-CO2 effects. Achieving the very ambitious goals of flying as CO2 neutral as possible and, in an ideal world, climate neutral, will require the design and development of highly efficient aircraft configurations and engines. In addition, the remaining climate impact of engine emissions, such as particles and water vapor in the atmosphere, must be reduced and, if necessary, offset by market-based measures in the sense of calculated climate neutrality.

Due to the physics of the atmosphere, the climate impact of aircraft is strongly dependent on the flight altitude [2, 3, 4] [e.g.]. Flying at lower flight altitudes often reduces the climate impact of contrails and NOx emissions. For reasons of efficiency and cost, current aircraft designs require certain flight speeds and associated optimum flight altitudes. Including a variation of Mach number and maximum flight altitude can identify additional potential savings in climate impact accompanied by an increase in operating costs [4]. Based on this exponential behavior, a trade-off between energy demand, economic efficiency and climate impact has to be found. The study is limited to the reduction of flight altitude and Mach number as a mitigation measure to reduce climate impact, and does not consider flying around localized regions where contrail formation is disproportionately high.

2. Market analysis of the long-range segment

The aircraft developed in this study are designed for long-haul flights. From a market and environmental perspective, the following questions arise:

- How many passengers (or passenger-kilometers) and flights are operated annually on long-haul routes, and what is their global share?
- Which long-haul routes have the most flights (departures), passengers and passenger- kilometers operated?
- Which long-haul routes have the highest CO2 emissions?
- Which aircraft fleets operate the most flights, passengers and passenger-kilometers on longhaul routes?
- What is their average seating capacity?

To answer these questions, the data analysis is carried out based on global flight movement data from the Sabre database for 2019 [5].

Table 1 – Comparison of passengers, revenue passenger kilometers (RPK), available seat kilometers (ASK) and CO2 emissions on all routes worldwide in 2019 and particularly on the long-haul segment (>4000km)

	Passengers	RPK	ASK	CO2	CO2/PaxKm
	[Mio]	[Billion]	[Billion]	[Mio Ton]	[g]
All routes	4.559 [5]	8.448 [5]	10.358 [5]	819 ¹	97
	4.500 [6]	8.686 [6]	10.541 [6]	785 [7]	
				778 [8]	
Long-Range	451	3.230	3.953	337 ¹	104
Share [%]	9.9	38.2	38.2	41.2	

¹CO2 calculations were carried out in this study using the CO2 emissions calculation model developed by ICAO [6].

The average seat occupancy, also known as the seat load factor (SLF) in the long-haul segment (Ih) is defined as:

$$SLF_{lh} = \frac{RPK}{ASK} = \frac{3230}{3953} = 0.817 \tag{1}$$

And for all routes as:

$$SLF_{allRoutes} = \frac{8.448}{10.358} = 0.816 \tag{2}$$

Further statistics on the top 5 long-haul routes in terms of passengers, passenger-kilometers, operations, CO2 emission density and the top aircraft types with the most seat-kilometers flown (ASK) are provided in the Appendix.

The mean of all average seats per operation, taking into account the corresponding ASK share, gives an average aircraft capacity for the entire long-haul segment of 312 seats. This is close to the typical number of seats in the A350-900 fleet (315)[9]. This indicates that the A359 would have a higher (and therefore superior) seat load factor than the other aircraft types in the Table 9 if the total passenger volume was served by only one of these aircraft types. The aircraft types with the highest transport volumes are the Boeing 777-300ER, Boeing 787-9, Airbus A380-800, Airbus A330-300 and Airbus A350-900. As the successor of the B777, the B777X, is not yet certified and the A380 and A330-300 are no longer in production (the A330-300 has been replaced by the A330-900), these three aircraft are not considered as reference aircraft for 2019. The two remaining aircraft, the B787-9 and the A350-900, offer a comparable maximum payload of 52-53 tons. The difference between the two aircraft is that they can transport this maximum payload over different distances: the A359 up to 5700 nm [9] and the B787-9 up to 5250 nm [10]. Looking at a specific route in the 6000 nm range, the A359 can carry significantly more passengers:

Max Payload:

- A359 50.3 tonnes
- B787-9 45.2 tonnes

For this reason, the A359 has a better coverage of the passenger transport requirement (RPK) over all route lengths than the B787-9 and is chosen as the reference aircraft for this study. The distribution of passenger volume as a function of payload flight distance is plotted in Figure 1.

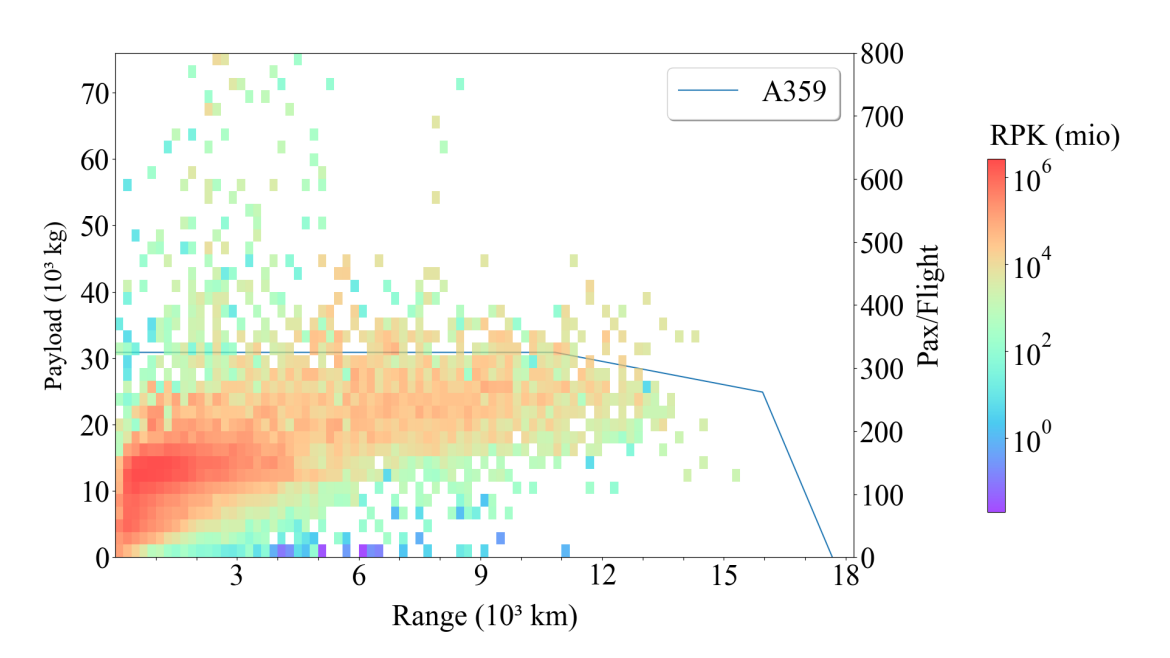


Figure 1 – Distribution of revenue passenger kilometer as a function of range and the superimposed payload range diagram of the Airbus A350-900 aircraft [9]

3. Methodology

The aircraft and engine design process is described in detail in the previous publication by Wöhler et al. [11] for the reference aircraft D325 as an Airbus A350-900similar aircraft [9] and the 2035 baseline aircraft fueled with kerosene, sustainable aviation fuel and liquid hydrogen designated D325+. The aircraft design process [12] that is integrated in the Remote Component Environment (RCE) [13] of the DLR comprises the DLR developed conceptual aircraft design tool openAD, the detailed engine performance map integration and scaling, the design mission calculation and the liquid hydrogen design sub-workflow described by Burschyk et. al [14]. For this study, the established aircraft design process is extended by the RCE-own design of experiments driver that varies the Mach number and altitude limitations to be discussed subsequently in Chapter 4.

For the design evaluation, the payload range characteristics, the mission simulation and emission calculation, climate impact assessment and cost assessment are connected downstream and are explained in detail below. A schematic overview of the aircraft design and evaluation workflow is depicted in Figure 2.

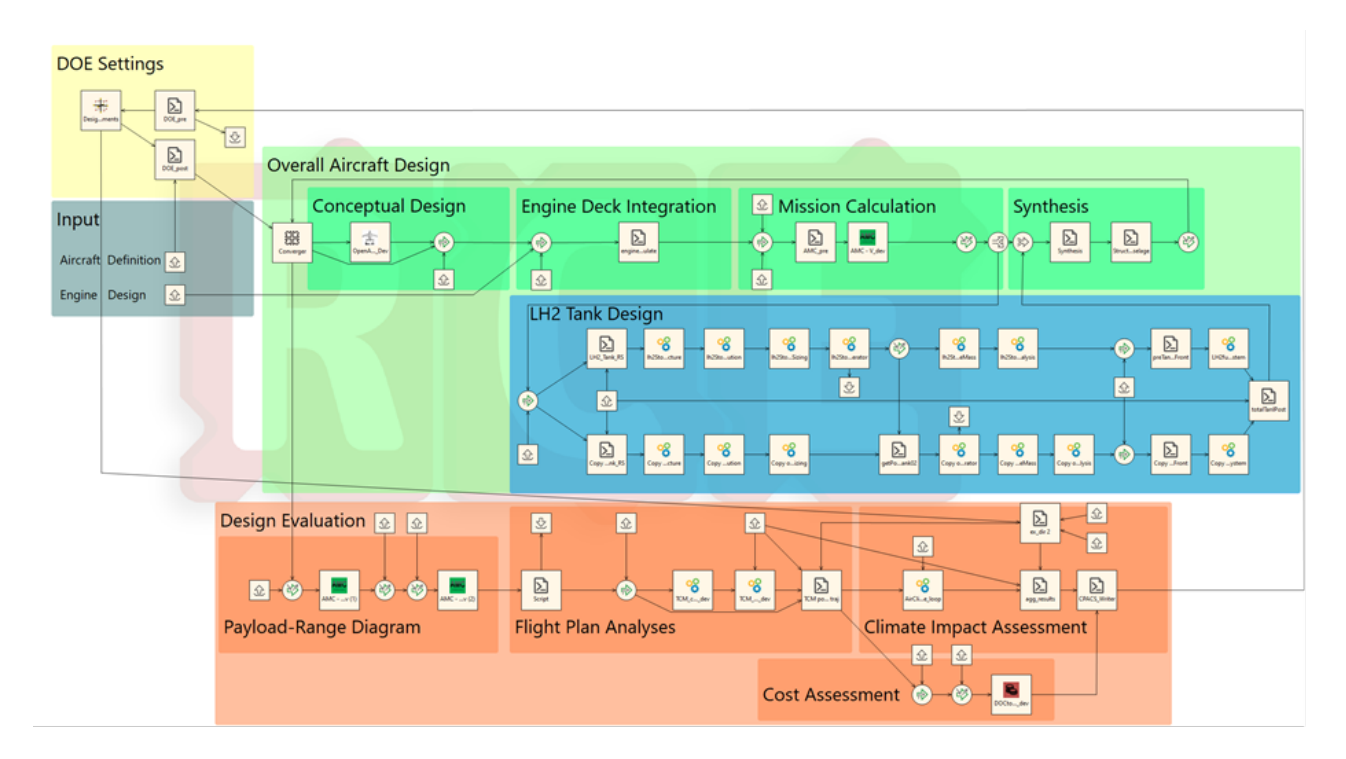


Figure 2 – A schematic representation of the design and analysis process in RCE [13]

3.1 Engine design and scaling

A multidisciplinary conceptual design process is used to design an engine for each fuel scenario. The engine requirements for each fuel scenario are adjusted according to the corresponding baseline aircraft design and the same set of technological assumptions is applied. An overview of the performance characteristics of the engines can be found in [11]. Thermodynamic differences are mainly related to different fuel heating values, exhaust gas compositions and the associated snowball effects during the engine design process. For each engine, thrust ratings are introduced and performance maps are calculated to be used during aircraft design. These engine performance maps are scaled in order to match the thrust requirements determined with the tool openAD within the applied iterative workflow. The engine thrust requirements are derived in the form of thrust-to-weight ratios at the following points: take-off, end of field and second segment (according to CS 25121 a and b), top of climb and cruise. The engine mass and the dimensions of the engine and nacelle are adjusted accordingly. However, no redesign of the thermodynamic cycle of the engine is done accounting for changes in thrust requirements or flight conditions at sizing operating points.

3.2 Engine emissions modelling

Engine emission scenarios are developed for each fuel scenario: kerosene (Jet-A1), sustainable aviation fuel (SAF) assuming 100 % synthetic paraffinic kerosene (SPK100) and hydrogen (H2). Table 2 shows an overview of the relevant fuel properties. The emission index (EI) relates the emitted mass or number of a species to the fuel mass burnt. Due to a significant reduction of aromatic compounds in the case of SAF, the synthetic fuel has a higher hydrogen mass fraction compared to kerosene. This increases the fuel heating value and the emission index for the species H2O (assuming complete combustion) but the emission index for CO2 is slightly lower in the case of SAF. Hydrogen has a fuel heating value approximately three times higher than kerosene and no CO2 is produced during combustion but a high emission index for H2O is obtained.

Table 2 – Overview of fuel properties that are assumed for the different engine models

Energy carrier		Kerosene	SAF	LH2
Heating value	[MJ/kg]	43.25	44.04	118.82
H2 mass friction	[%]	13.8	15.3	100
EICO2	[kg/kg]	3.156	3.104	0.0
EIH20	[kg/kg]	1.239	1.367	8.937

The indices for nitrogen oxides (NOx) and non-volatile particulate matter (nvPM) emissions depend not only on the fuel but also on the combustion chamber technology used, the thermodynamic boundary conditions and the technological maturity of the combustion chamber design. Here, NOx and nvPM emissions are predicted using correlation-based models, which were calibrated according to data of existing combustion chambers published in the ICAO engine data bank (ICAO EDB v28C). NOx emissions are modeled by means of the p3-T3-method according to [15] as applied in [16]. Non-volatile particulate matter emissions are predicted by means of the Döpelheuer method [17, 18]. An rich-burn, quick-mix, lean-burn combustion chamber concept was assumed for all engines in this study. For the reference engine, the model was calibrated using the ICAO emission characteristics of the Trent XWB and for the baseline configuration, the ICAO data for the Talon X combustor of the PW1100G was used.

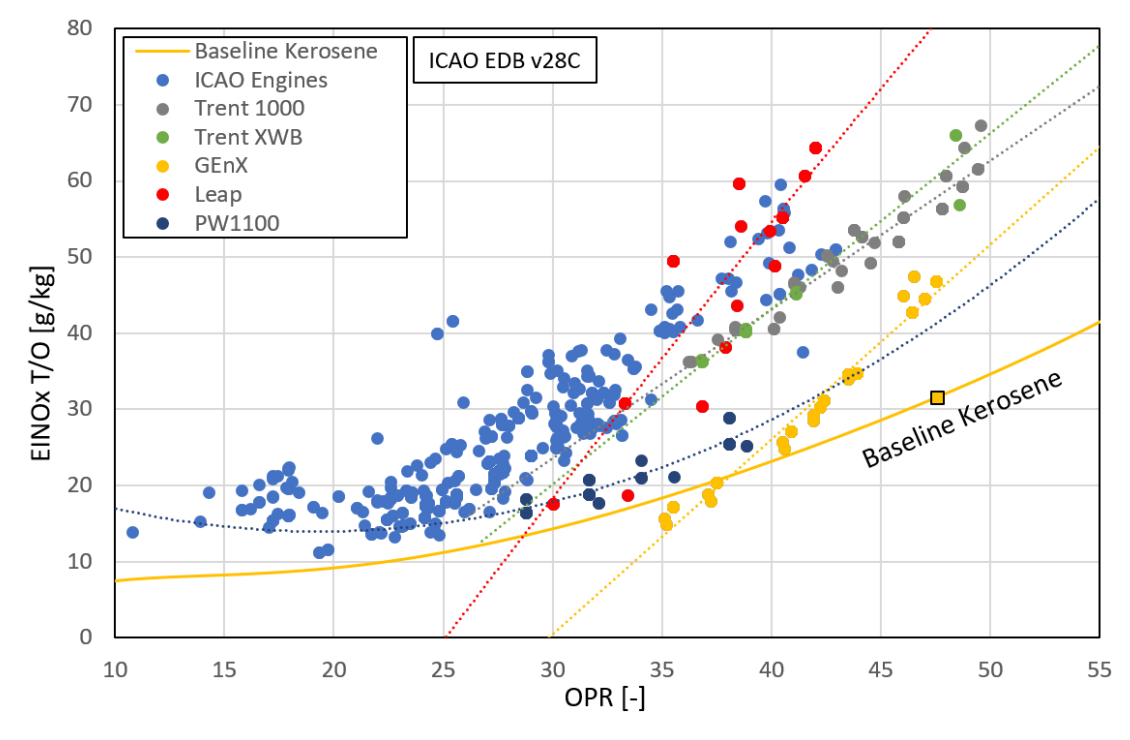
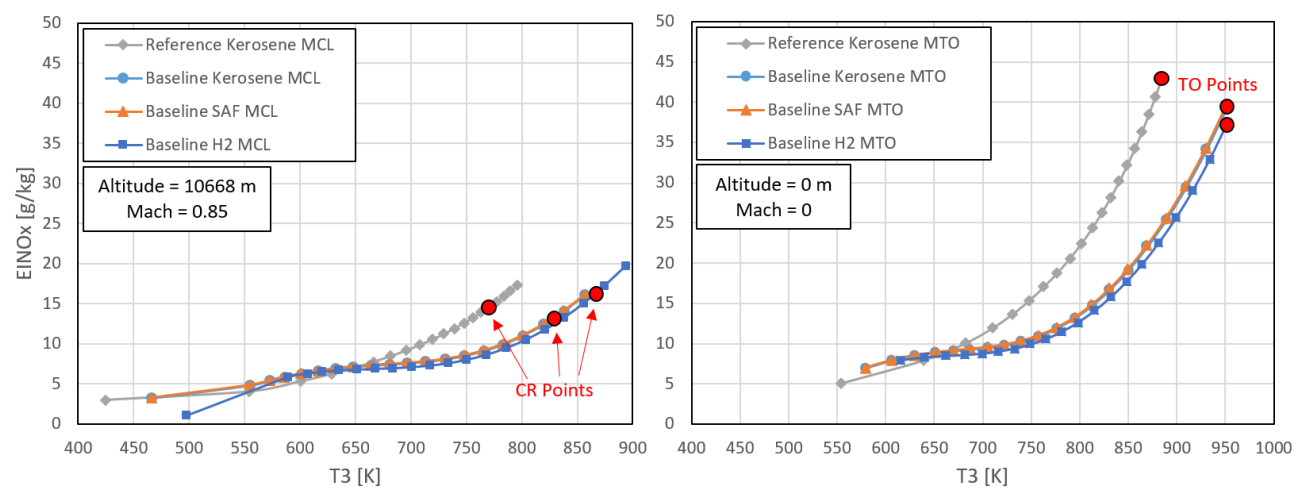
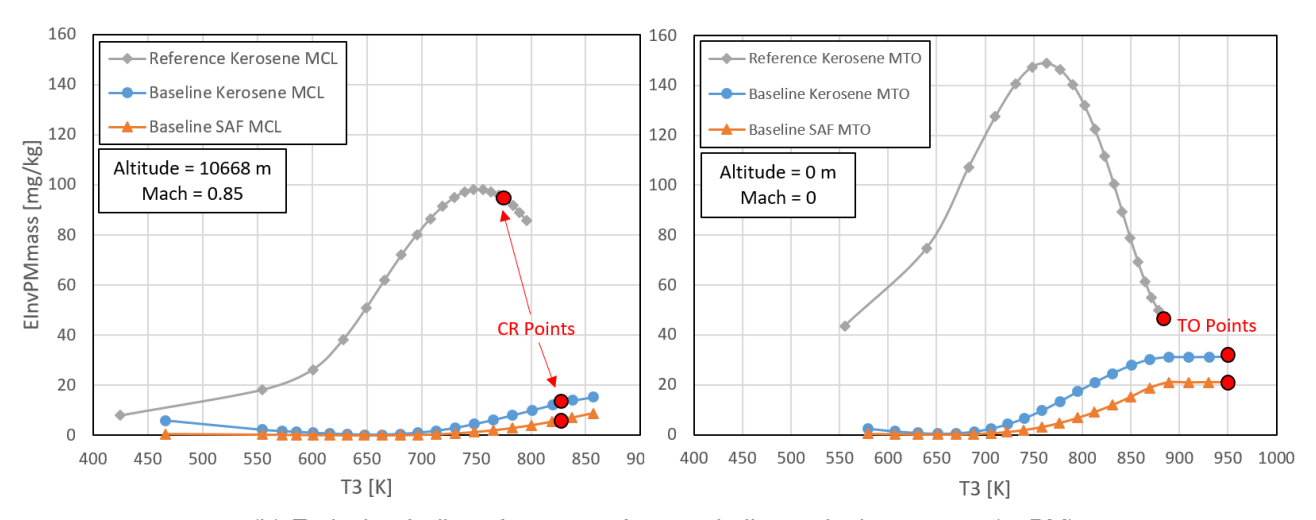


Figure 3 – Emission index for NOx of the baseline engine model (kerosene) compared to ICAO data of real existing engines for the operating condition T/O at sea level static (SLS) conditions

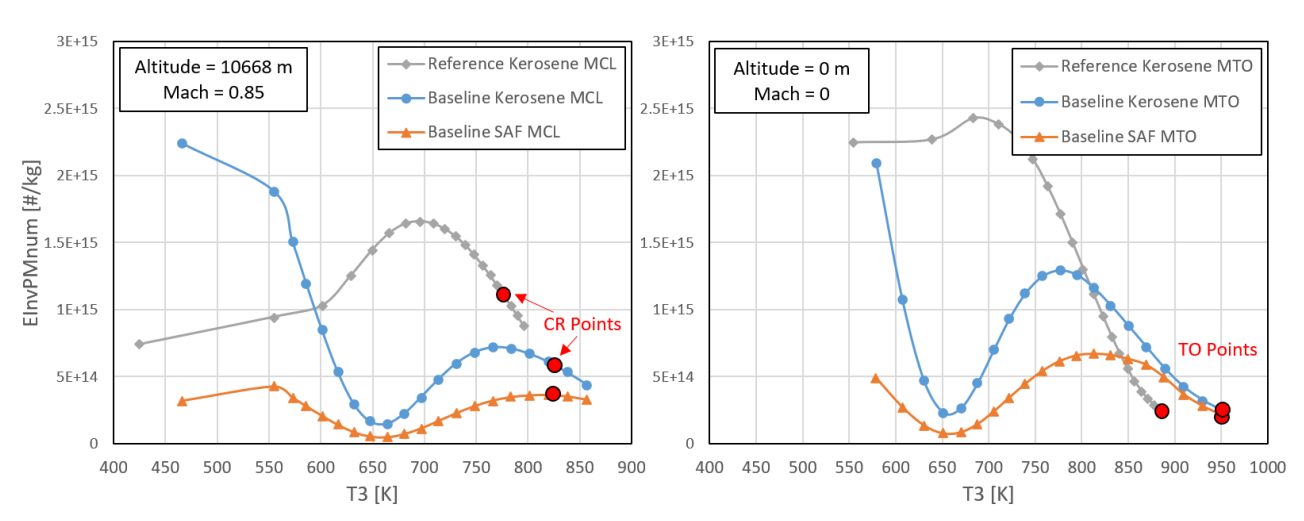
Climate Impact and Economic Assessment of LH2 and SAF Long-Range Aircraft Concepts



(a) Emission Indices for Nitrogen Oxides (NOx)



(b) Emission Indices for mass of non-volatile particulate matter (nvPM)



(c) Emission Indices for number of non-volatile particulate matter (nvPM)

Figure 4 – Load-dependent emission characteristics of the engine models for the maximum climb rating (MCL) at cruise flight conditions and for the maximum take-off rating (MTO) at sea level static (SLS) conditions as a function of the combustor inlet temperature (T3)

Figure 3 shows the emission indicies for NOx of the baseline engine model at sea level static (SLS) for the operating condition T/O in comparison with ICAO data. Starting with a characteristic similar to the ICAO data of the PW1100G, adaptions are made to account for changes in the thermodynamic

cycle as described in [16]. Additionally, a reduction of 10 % in NOx and nvPM emissions is assumed to account for an entry into service in the year 2035 resulting in the yellow solid line and the corresponding T/O operating point for the kerosene baseline. It should be noted that NOx emissions increase with increasing OPR, i.e. a direct comparison of engines for different OPRs is not permissible. Compared to state-of-the-art technology, a significant reduction in NOx emissions is assumed for the baseline engine. However, predicting NOx emissions for future combustors is highly uncertain and the models applied here rather show a plausible future scenario and are not a precise prediction of future emission levels.

With respect to absolute NOx emissions, it is assumed that there is no difference between the combustion of kerosene and SAF. In consequence, the emission index EINOx is slightly higher for the SAF scenario: a higher fuel heating value of SAF compared to kerosene leads to less fuel mass flow that is required for producing the same thermal output. For the combustion of hydrogen, the achievable level of NOx emissions using a RQL-combustor is assumed to be similar to kerosene and the same emission characteristic is used. Secondary effects that have an influence on operating pressure and temperature of the thermodynamic cycle as e.g. the exhaust gas composition are taken into account by using the emission models.

The nvPM emissions are modeled for kerosene and SAF since the concentration of particles in the engine's jet has an influence on the formation of condensation trails and related contrail induced cloudiness. Therefore, the particle number is an required input for the atmospheric model that is derived from the nvPM mass by modelling an average particle diameter in dependence on engine load. For the SAF scenario, the nvPM emissions are significantly lower compared to kerosene, as there are fewer aromatic compounds contained in the fuel. The particle reduction compared to conventional kerosene depends on the load condition and is between approx. 30% and 90%. The highest reductions are achieved at low load. In the case of hydrogen, a no carbon-containing fuel is burned and no nvPM emissions are expected as a result of combustion.

Figure 4 shows the emission characteristics for NOx as well as the mass and number of nvPM for the reference engine and the baseline engines for ground and altitude conditions as a function of the engine's load condition given by combustor inlet temperature (T3).

3.3 Mission simulation and emission calculation

This section provides a detailed description of the process from initial mission analysis of an aircraft design to the final calculation and spatial distribution of emissions for climate impact assessment. At the beginning of the mission analysis, the payload range diagram and fuel consumption for a characteristic evaluation mission are calculated for the respective aircraft designs in the Aircraft Mission Calculator (AMC) by solving the equation of motion at any defined time step. Based on the results, aircraft performance can be estimated and compared at aircraft level prior to detailed trajectory simulations. For the payload range diagram, in addition to the design mission, the characteristic key points are analyzed. These include the maximum range with maximum payload, the range with maximum fuel mass and the ferry flight without payload.

Based on these results, the next step is to analyze the developed flight plan. A total of 3209 flights are included in the mission simulation, representing flights above 4000 km in 2019 as illustrated in Figure 5. For each aircraft configuration from the aircraft design, these missions are calculated using the great circle distance for each origin-destination pair. This is the basis for the detailed trajectory simulations, where the Trajectory Calculation Module (TCM) is employed to calculate detailed emission inventories using 4D trajectories[19, 20]. TCM performs fast-time simulations by integrating relevant flight conditions through a total energy model. It processes mission parameters, aircraft mass breakdown, and engine and aerodynamic performance tables for various flight conditions. This capability allows for the simulation and evaluation of flight performance for all designed aircraft configurations. The configurations are handed over using the CPACS file format after a design and evaluation missions have been successfully calculated during aircraft design and a payload-range diagram is obtained, as described above. For this comparative study, the simulation focuses on the effects of long-distance flights, starting and ending at an altitude of approximately 1500 meters. Takeoff and landing phases are not accounted for, as the study aims to isolate and evaluate the impacts of cruise altitudes and Mach number variations on emissions and climate metrics.

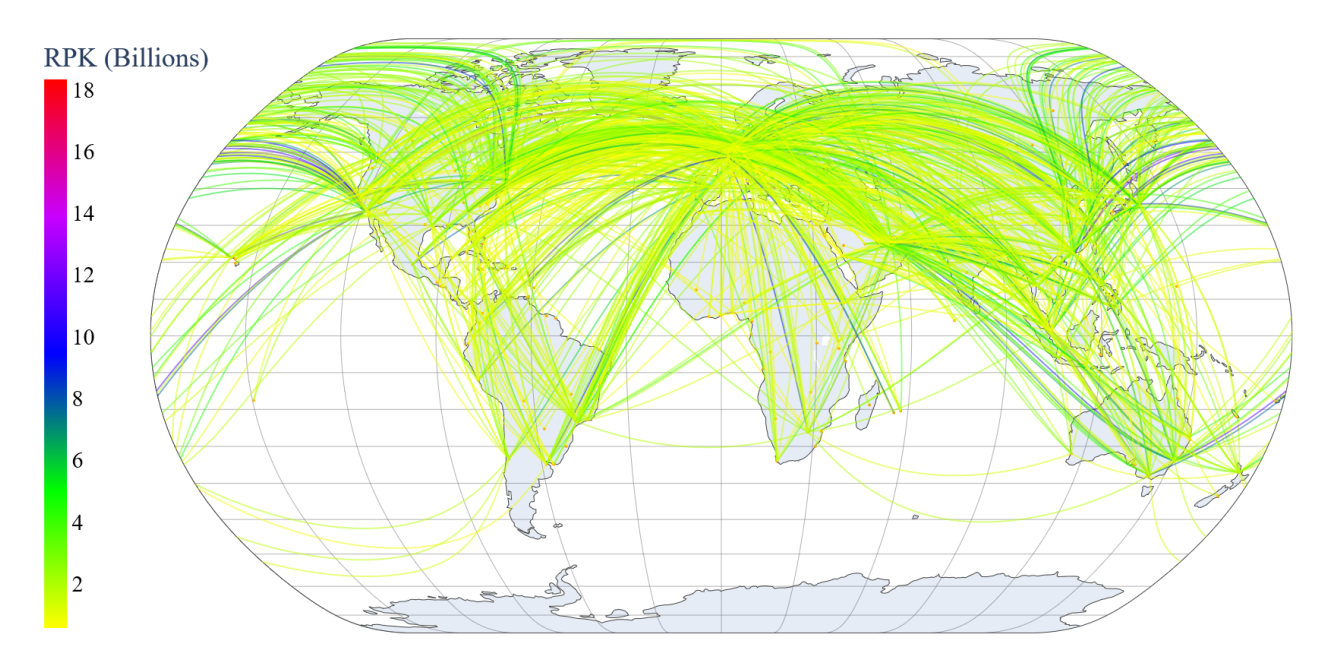


Figure 5 – Illustration of the 3209 origin-destination pairs as a function of revenue passenger kilometer computed for each aircraft configuration

Emissions for each aircraft configuration for each flight in the established flight plan are calculated using TCM and are spatially distributed on a numerical grid. This facilitates detailed climate impact assessments based on the gridded output.

3.4 Climate assessment

The climate impact of an emission can be analyzed and quantified in detail using a complex three-dimensional climate-chemistry model that takes all atmospheric processes into account. However, as this is very computationally intensive and requires several weeks on a supercomputer, it is necessary for certain applications to calculate the climate impact using a simplified model, e.g. a climate response model. In contrast to the climate-chemistry model, which includes all processes, a response model only maps the response, i.e. the effect of the emission on the radiative forcing and the temperature, whereby the individual processes are no longer investigated.

In this study, the climate response model AirClim [21, 22] is used to calculate the climate impact of aviation emissions. AirClim combines precalculated atmospheric responses (effect per emission) with the location-dependent emissions to calculate the climate impact. Different idealized emission regions (latitude and altitude) were defined for the precalculated response. For each of these emission regions, a climate-chemistry simulation with normalized emissions of nitrogen oxides and water vapour was carried out to simulate the atmospheric response of this emission. Concentration changes of ozone and water vapor, lifetime changes of methane and their radiative forcing were calculated with the climate chemistry model E39/CA (e.g. [23]). Simulations with ECHAM-CCMod [24] were used for contrail induced cloudiness (CiC). The results of these simulations are used in AirClim as response surfaces. AirClim combines these height- and latitude-dependent response surfaces with the 3D emission maps to calculate the concentration changes, radiative forcing and near-surface temperature change. A more detailed description can be found in [21] and [22].

In this study ATR (Average Temperature Response) with a time horizon of 100 years and constant emissions over a typical aircraft lifetime of 28 years is used as a climate impact metric. ATR100 indicates global near surface temperature change averaged over 100 years:

$$ATR100 = \frac{1}{100} \int_0^{100} \Delta T(t) dt.$$
 (3)

This metric has already been used in some other technology assessments [22, 25].

3.5 Economic assessment

For the calculation of operating costs, the modeling according to Thorbeck [26] is applied and extended by the component and system cost estimation according to Beltramo [27]. The method provides a simplified approach to the determination of direct operating costs (DOC) at aircraft level, taking sufficient account of the relevant parameters. The cost terms thereby are corrected by currency exchange rates and inflation. The annual DOC are composed of fees, maintenance costs, crew costs, and the cost of the aircraft itself. This assumption is sufficient for the evaluation of aircraft with comparable architectures. However, the component masses in the design of a hydrogen-powered aircraft differ more significantly from those of a kerosene powered aircraft, so these must be considered in detail. This adaptation of the methodology is documented in [28] and [29]. For the estimation of the capital costs for the hydrogen designs, an additional price of 350 €/kg for the tank structure and 1500 €/kg for the hydrogen systems based on the studies of [27] is considered.

3.6 Cost of the energy carrier options

The historical development of Jet-A1 fuel prices on the U.S. Gulf Coast (kerosene-type jet fuel) [30] from April 1990 to October 2022 is used to estimate fuel costs. Scenarios for future fuel price development are taken from the Annual Energy Outlook (AEO), an annually published forecast for the energy sector up to the year 2050 from the U.S. Energy Information Administration (EIA). The most recent report is AEO 2022, published on March 3, 2022. The AEO forecast contains a reference forecast as well as a scenario for low and high kerosene price development [30]. The conversion factors for barrels to tons are assumed to be 0.127 [31] and Dollars to Euros at the average exchange rate for 2021 (0.85). The fuel prices are shown in Euros per gigajoule (€/GJ) for the estimation of the DOC.

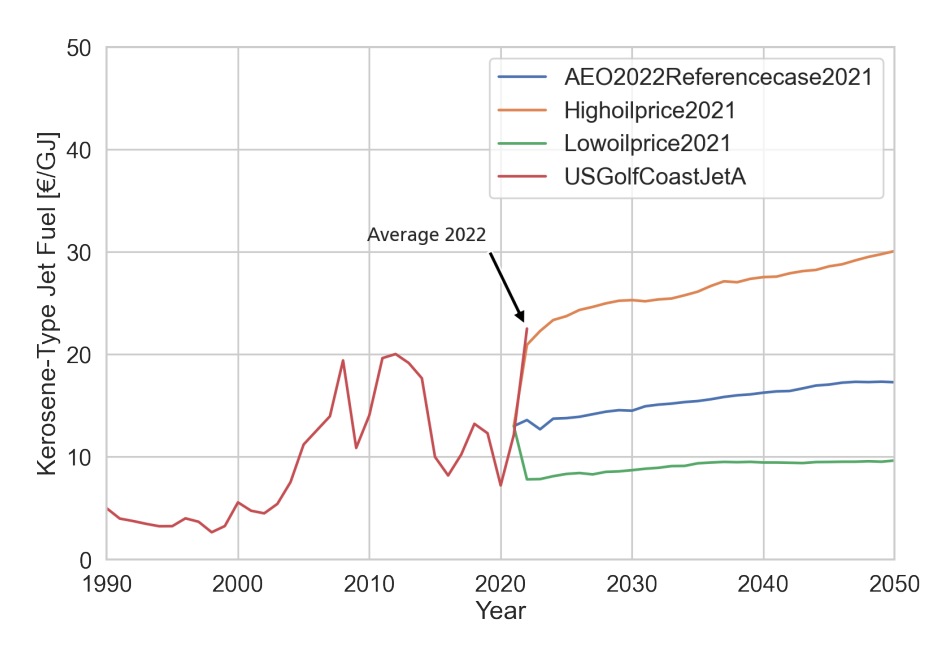


Figure 6 – Cost trends and forecasts for kerosene-type jet fuel according to [30] and [31]

The identified US Gulf Coast spot price in 2021 is 12.1 €/GJ, while the AEO assumes 12.9 €/GJ for the reference year as depicted in Figure 6. The annual average price of US Gulf Coast Jet-A1 (until October 2022) is already higher than the AEO's "high oil price 2021" scenario. The average price of Jet-A1 over the last ten years is 13.7 €/GJ. The energy price is therefore driven by external factors and is highly volatile. As a point of comparison, a kerosene price of 15 €/GJ is chosen as the reference scenario for 2035, based on the AEO2022 reference case. Price estimates for SAF and LH2 are beyond the scope of this study and estimates vary widely depending on the assumptions made. Therefore, different price levels are examined, set at 15 €/GJ, 30 €/GJ, 45 €/GJ and 60 €/GJ, to generate generic test cases that highlight the impact of fuel prices on the DOC of different energy carrier options.

4. Aircraft design and assessment

In order to establish and evaluate the comparison point for the different energy carrier options, the baseline designs scenario at Mach number 0.85 and maximum flight altitude of FL430 for 2035 described by Wöhler et. al. [11] are evaluated first in terms of economics in regard to DOC and climate impact in regard to the average temperature response of the ATR100. The design process for altitude and Mach number variation is then described and evaluated to identify the additional climate impact potential and associated costs. These are compared with the baseline designs for 2035.

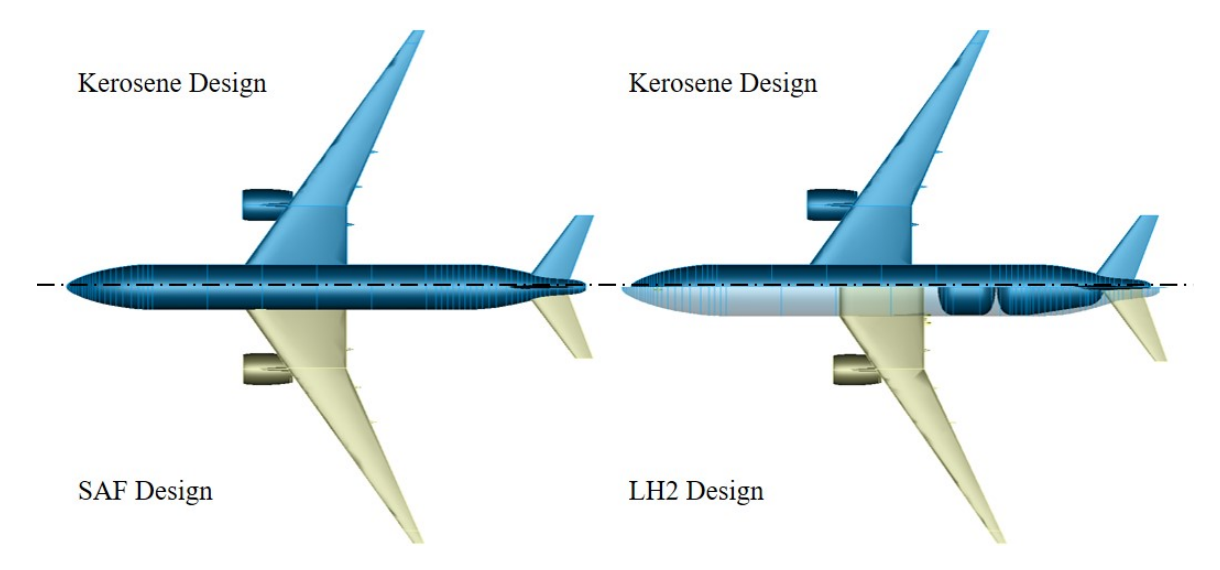


Figure 7 – Geometric top view comparison of the D325+ baseline aircraft designs for kerosene, SAF and LH2 retrieved from [11]

Table 3 – Key characteristics of the D325+ baseline aircraft designs for Kerosene, SAF and LH2 as energy carriers on long-range application in comparison to the D325 reference aircraft retrieved from [11]

		D325	D325+ Kerosene		D325+ SAF		D325+ LH2	
Masses								
MTOM	[kg]	280000	273115	-2.5%	269701	-3.7%	232401	-17.0%
MLM	[kg]	206800	205242	-0.8%	204375	-1.2%	213784	3.4%
MZFM	[kg]	195600	194778	-0.4%	194303	-0.7%	210914	7.8%
OEM	[kg]	141700	140928	-0.5%	140453	-0.9%	157064	10.8%
MFM	[kg]	113400	103314	-8.9%	100593	-11.3%	35463	-68.7%
Block fuel (4000 nm)	[kg]	45994	43630	-5.1%	42473	-7.7%	16058	-65.1%
Block energy (4000 nm)	[GJ]	1989.2	1887.0	-5.1%	1870.9	-5.9%	1908.0	-4.1%
Propulsion								
Equivalent static thrust (Sea-level/ISA)	[kN]	374.8	360.3	-3.9%	360.3	-3.9%	295.6	-21.1%
TSFC cruise (mid cruise/ISA/Ma=0.85)	[g/kN/s]	15.23	14.70	-3.5%	14.45	-5.1%	5.13	-66.3%
TSEC cruise (mid cruise/ISA/Ma=0.85)	[J/N/s]	658.90	635.97	-3.5%	636.52	-3.4%	609.55	-7.5%
Aerodynamics								
Sref	[m²]	445	421	-5.4%	414	-7.0%	353	-20.7%
cLmaxL	[-]	2.15	2.36	9.8%	2.36	9.8%	2.8	30.2%
cL (mid cruise/Ma=0.85)	[-]	0.433	0.469	8.4%	0.47	8.5%	0.469	8.4%
L/D (mid cruise/Ma=0.85)	[-]	20.57	20.87	1.5%	20.9	1.6%	19.24	-6.5%

A top view comparison of the baseline designs is shown in Figure 7. For the fossil kerosene and SAF designs, the difference is limited to the lower heating and density of the fuel, thus both configurations are nearly identical and differ only slightly in the required size of the wings. For hydrogen, a 12-abreast cabin and fuselage design is derived with both hydrogen tanks in the rear. Table 3 highlights the key characteristics of the three aircraft configurations as derived in [11].

4.1 Climate impact and direct operating cost assessment of the baseline designs

The climate impact of the Jet-A baseline is dominated by the effect of CiC, which causes around 44% of the impact as depicted in Figure 8. 28% is caused by NOx, which is composed of the effect of ozone and methane. CO2 causes about 23% of the effect while H2O is only about 5%. If SAF is used instead of Jet-A, the overall effect is reduced by around 30%. The main reason for this is the assumption that SAF is CO2 neutral, which reduces the overall effect by 23%. In addition, the reduction in particulate emissions leads to a reduction in the CiC effect of around 20%, which results in an additional reduction in the overall effect of around 10%. For the LH2 aircraft design in comparison to the Jet-A1 variant, the climate impact is reduced by around 50%. This is achieved by the lack of effect of CO2 emissions and the reduced effect of CiC due to the strong reduction in particulate emissions.

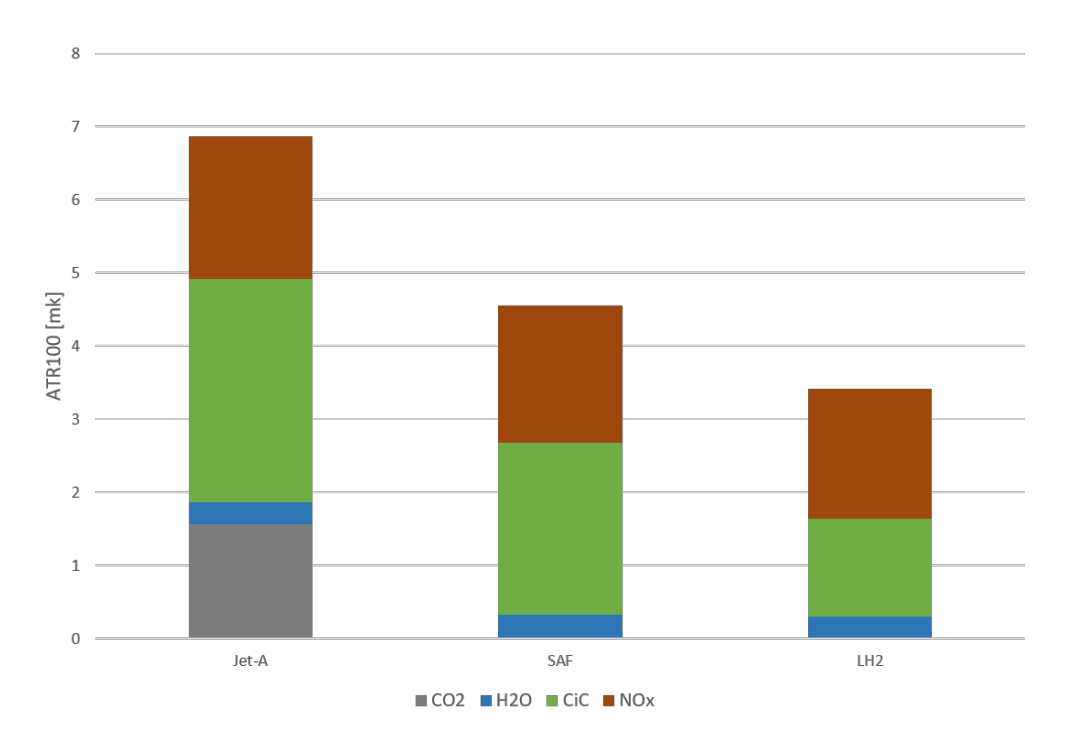


Figure 8 – Comparison of the climate impact in terms of ATR100 of the baseline designs for Jet-A1, SAF and LH2 and Mach 0.85 and a maximum flight altitude of 43 kft

The direct operating costs for the different aircraft designs presented in Figure 9 follow a similar trend for all designs, as the costs are dominated by the fuel and capital fractions under the assumption that the fuel price for all three energy carriers is the identical. This assumption is made as it was beyond the scope of this study to develop a specific price scenario and to highlight the impact of the aircraft designs directly. Figure 15 depicts the impact of generic fuel prices on the DOC. Fuel costs account for about 30%, while the capital cost split, which consists of recurring costs and profit, is slightly higher at about 34%. The third largest contributor to the DOC, at approximately 18%, are aircraft fees, which consist of air traffic control (ATC), ground handling and landing fees. Maintenance costs for engine and airframe material and personnel account for about 10% of the total DOC. Crew costs represent the smallest portion of the annual DOC and are identical for all three aircraft designs, given the same number of pilots and flight attendants and the same number of crews per aircraft per year, since the number of passengers is consistent.

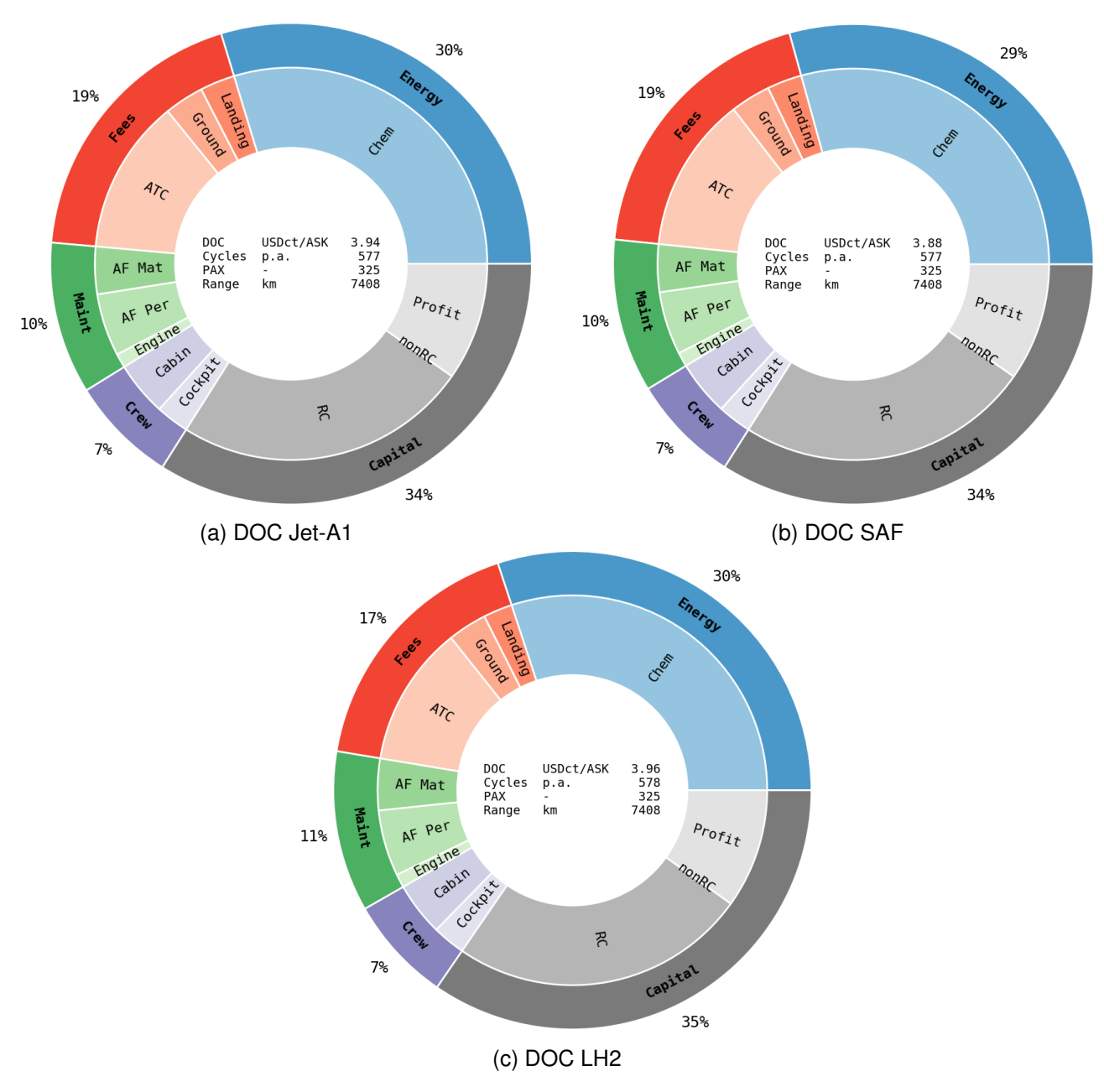


Figure 9 – Split of the annual direct operating cost of the aircraft designs for Jet-A1, SAF and LH2 and Mach 0.85 and a maximum flight altitude of 43 kft on the evaluation mission of 4000nm (7408km) and a constant fuel price of 15 €/GJ.

Since the SAF aircraft design is slightly more efficient than the Jet-A1 aircraft on the 4000nm evaluation mission, as can be noted from Table 3, due to the SAF's higher lower heating value and therefore less fuel mass required, the DOCs are slightly lower by 1.5%. A detailed description of the aircraft design rationale is given in [11]. The evaluation mission represents a typical mission for the long range market segment. The DOC of the LH2 aircraft design differs slightly more from the kerosene-type aircraft designs, while the total cost is marginally higher by 0.5% compared to the Jet-A aircraft. Since the maximum take-off mass (MTOM) of the LH2 aircraft is lower than that of the other two designs (see table 3), the charges are lower as the MTOM has the main impact on ATC and handling. The maintenance costs are higher by 1% because the hydrogen tank and system must be maintained, and the capital costs are also higher by 1%. These are related to the hydrogen tank and system as well as the larger fuselage but smaller wing, which can be noted in the table 3 as part of the Operating Empty Mass (OEM). Assuming identical energy-specific prices for all fuel types, there is no difference in fuel cost, as both aircraft require almost the same amount of block energy to fly the evaluation mission.

4.2 Mach number and altitude variations

In the scope of this paper, parameter studies are conducted by automatically varying the design Mach number and the maximum permissible flight altitude to reduce the climate impact. A customized aircraft configuration is designed for each combination of these parameters.

All configurations are designed as conventional low-wing and tube configurations with two engines mounted under the wing. A maximum wingspan of 64.8 m or, for structural reasons, a maximum aspect ratio of 12.5 are taken into account when dimensioning the wing for the purposes of airport integration. To determine the maximum lift, Fowler flaps with a single gap are assumed for all designs. The sweep of the wing, the camber and the airfoil thickness are adjusted according to the design Mach number. As the Mach number is reduced, the sweep angle decreases, which leads, among other things, to better high-lift coefficients assuming the same architecture of the high-lift system. The tail units are designed on the basis of constant volume coefficients for this aircraft class.

The wing area is determined on the basis of the required low-speed flight characteristics and the take-off and landing distance. Furthermore, it is assumed for kerosene and SAF configurations that the entire fuel is accommodated in the wing and center wing box. This leads to a corresponding boundary condition for the wing volume and thus the wing area. For LH2 configurations, the tanks are integrated into the back of the fuselage so that the fuselage geometry is adapted to the requirements of the tank size and the boundary condition for the wing volume does not apply. The detailed hydrogen aircraft design was described in [11].

Table 4 – Flight altitude and Mach number range

Parameter	Unit	from	to
Mach number	[-]	0.7	0.85
Maximum flight altitude	[ft]	25000	43000

The parameter study vary the design Mach number and the upper limit of the flight altitude as summarized in Table 4. The Mach number is reduced in 0.05 increments from Mach 0.85 to Mach 0.7. The flight altitude limit is reduced in 3000 ft increments from 43000 ft to 25000 ft. A turbofan engine architecture is assumed for all designs, while a turboprop architecture may have been superior in terms of efficiency, especially at lower Mach numbers, but was beyond the scope of this study. Not all of the above combinations lead to convergence during aircraft design or flight path evaluation. In error cases, the Mach number was varied by +/-0.01 to improve convergence behavior and hence to provide the amount of data necessary for a feasible evaluation. As a consequence, the individual results show a variation in the distribution, but represent the Pareto fronts in the final evaluation in a meaningful way. An overview of all converged aircraft configurations is given in Figure 10.

Figure 11 illustrates the representative results of Jet-A1 configurations for the cost scenario of 15 €/GJ as described in Chapter 3. The graph shows the relative deviation in DOC over the relative deviation in ATR100 related to the kerosene baseline. The variation of the flight altitude constraints and the adaption of the flight Mach number leads to a Pareto-front distribution of configurations. The climate impact can be traded against the costs. The graph illustrates that a reduction in altitude tends to reduce the climate impact. This is primarily caused by the lower effect of ozone (O3) and CiC (contrail induced cloudiness). At the same time, configurations can be identified that also appear to reduce the climate impact, if the altitude limit remains the same. In such cases the reduction in climate impact is primarily achieved by slower configurations. Since the mission analysis tools optimize the flight altitude to minimize fuel consumption, the altitude limit is not necessarily exploited by all configurations. Especially slower configurations try to avoid unreasonably high lift coefficients at cruise conditions by operating at lower altitude. Therefore, the same flight altitude limit does not necessarily mean the same flight altitude and vice versa. This results in partially identical configurations despite different altitude limitations, as only one design mission is used. However, the changed flight altitude limitation for off-design missions, as they mostly occur in the flight plan, can lead to different flight trajectories and thus to differences in costs and climate impact. With the configurations considered, a reduction in climate impact of up to 40% can be achieved in conjunction with a cost increase of up to 15%.

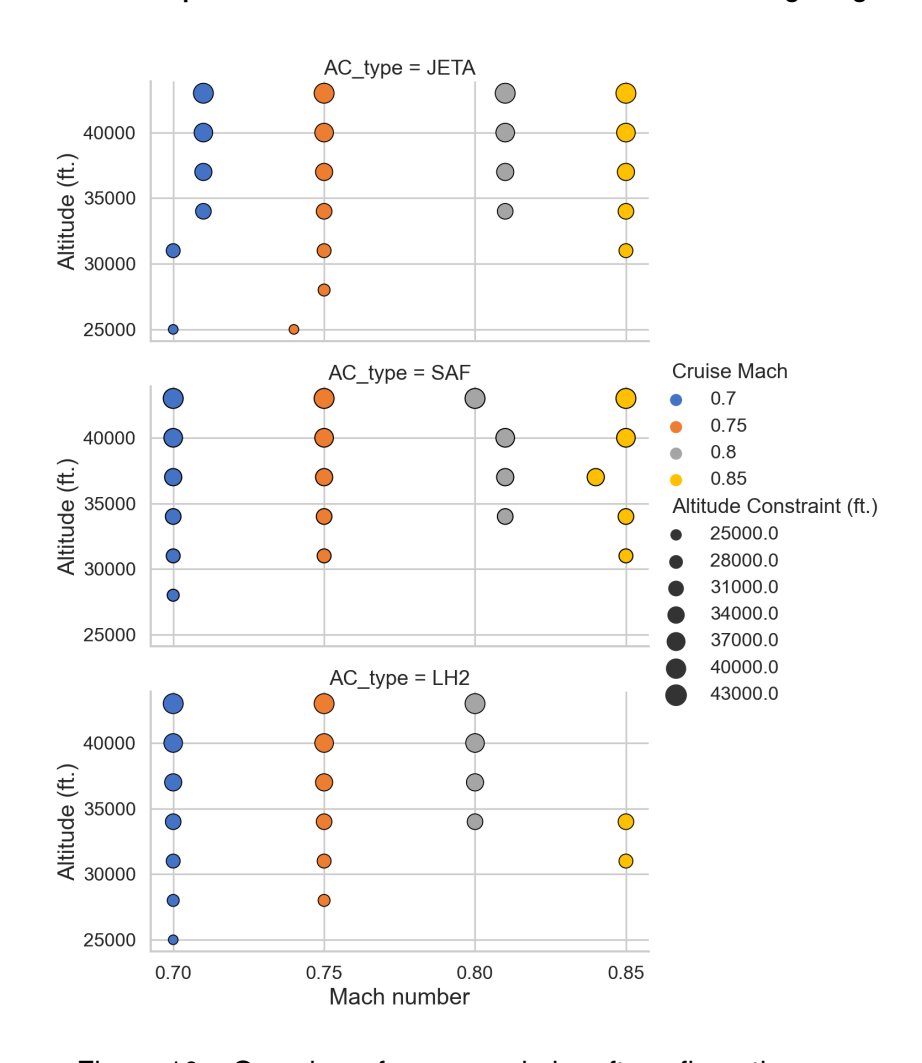


Figure 10 – Overview of converged aircraft configurations

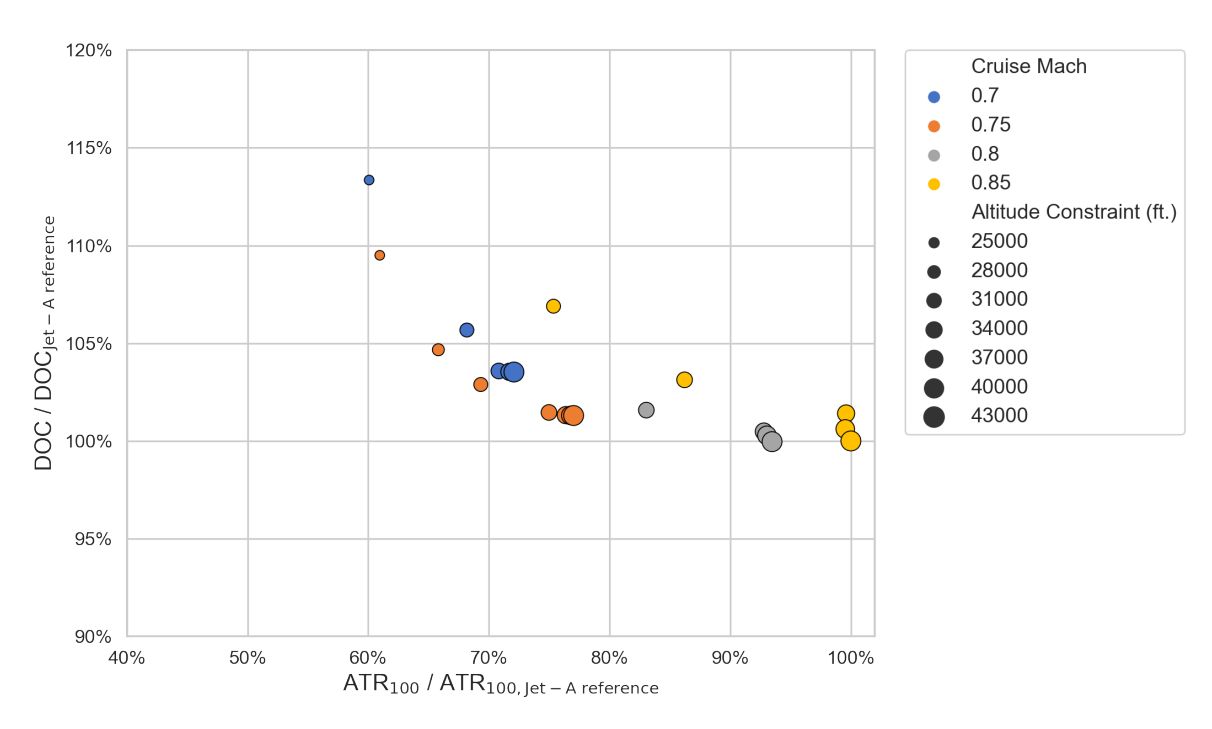


Figure 11 – Parameter study kerosene configurations: relative change of DOC over relative change of ATR100, related to the kerosene baseline configuration (Mach 0.85, flight altitude limit 43 kft).

Results for constant fuel costs of 15 €/GJ.

4.3 Jet-A1-Configurations

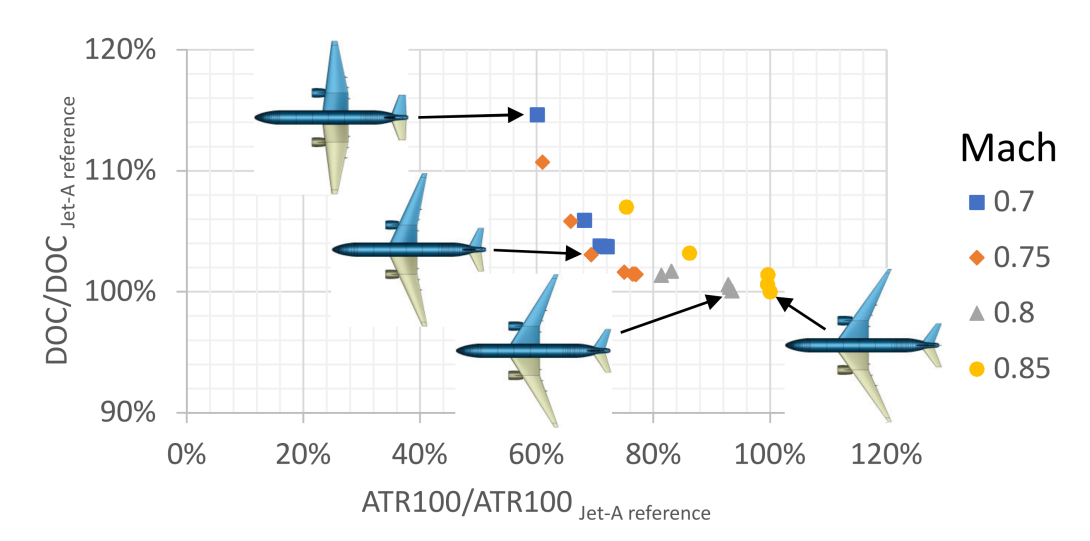


Figure 12 – Parameter study kerosene configurations: relative change of DOC over the relative change of ATR100, related to the kerosene baseline configuration (Mach 0.85, flight altitude limit 43 kft), distribution of design Mach numbers highlighted in color

The influence of the flight altitude limits and the design figures for the kerosene-powered configurations is shown in the Figure 12 above. The quantitative results refer to the Jet-A1 baseline for Mach 0.85 and a flight altitude limit of 43 kft. To illustrate the impact of the design parameters on the aircraft geometry, the top views of four representative configurations are integrated into the diagram. Clearly, the reduction in wing sweep with decreasing Mach number can be observed. Despite the improved maximum lift performance of configurations with a small wing sweep angle, the wing area is not reduced due to the fuel volume constraint.

When using Jet-A1, the climate impact can be reduced by up to 40% by changing the flight altitude and Mach number. Although this increases fuel consumption and thus CO2 emissions, this is more than compensated by the reduction of the climate impact of CiC. The effect of water vapour (H2O) is also significantly reduced at lower flight altitudes, but the contribution to the overall effect is small. The effect of NOx emissions also generally decreases with decreasing flight altitude, but is largely compensated for by the increase in NOx emissions due to increased fuel consumption. The increased fuel consumption and significant higher flight times at reduced Mach number lead to an decrease in flight cycles annually and thus increase in DOC of up to 15%.

4.4 SAF-Configurations

The influence of the flight altitude limits and the design Mach numbers for the SAF configurations is shown in Figure 13. The quantitative data is related to the SAF baseline for Mach 0.85 and a flight altitude limit of 43 kft. Representative top-views of four configurations along the Pareto-front are also depicted in the diagram.

When using SAF, the climate impact can be reduced by up to 50% compared to the reference mission by changing the flight altitude and flight speed. Since we consider SAF as CO2 neutral in this study, as only CO2 is emitted that was previously extracted from the atmosphere, the additional emission of CO2 for lower flight altitudes does not lead to an increase in climate impact. This leads to a higher overall savings potential. In terms of DOC the cost inceare by up to 9%. Compared to the Jet-A1 configurations, the aircraft design and flight path analysis did not converge for the lowest altitude constraints at the lower Mach numbers. Thus, the SAF is not more cost effective to operate than the Jet-A1, as could be inferred, but the corresponding data point is missing for SAF. At lower altitudes, the climate impact potential of the SAF could be further increased at higher DOC.

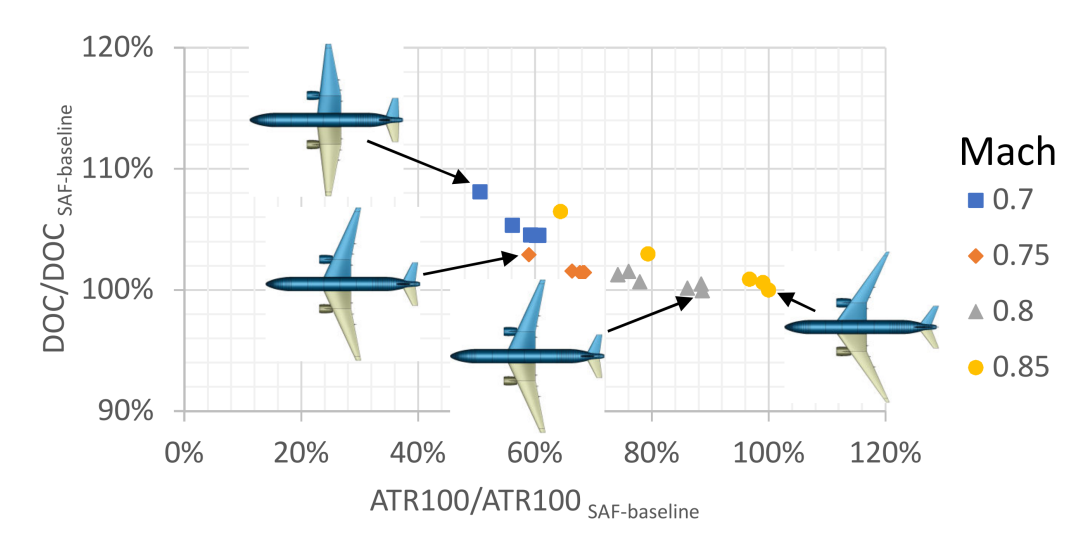


Figure 13 – Parameter study SAF configurations: relative change of DOC over the relative change of ATR100, related to the SAF baseline configuration (Mach 0.85, flight altitude limit 43 kft)

4.5 LH2-Configurations

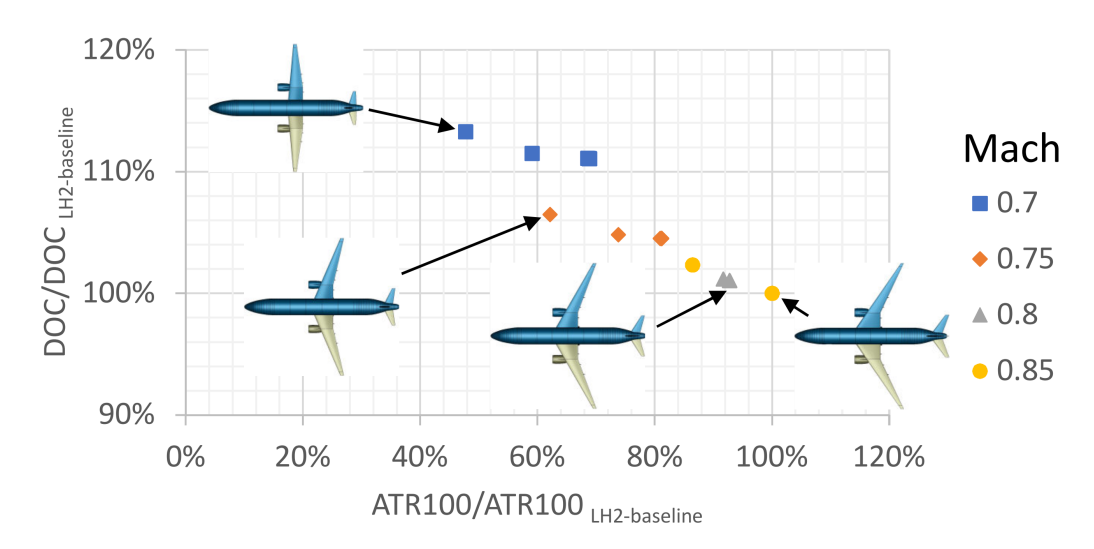


Figure 14 – Parameter study LH2 configurations: relative change of DOC over the relative change of ATR100, related to the LH2 baseline configuration (Mach 0.85, flight altitude limit 34 kft)

The influence of the flight altitude limits and design Mach numbers for the LH2 configurations is shown in Figure 14. The quantitative data here refer to the LH2 baseline for Mach 0.85 and an upper altitude limit of 34 kft. (Configurations with a higher ceiling above 34 kft km did not provide a sufficient amount of data for post-processing evaluation).

When using LH2, the climate impact can be reduced by up to 52% compared to the reference mission by changing the altitude and speed for the available data points. Since LH2 does not emit CO2, the additional emission of CO2 at lower altitudes does not increase the climate impact. The increase in DOC for the LH2 aircraft is steeper compared to the Jet-A1 and SAF configurations due to the greater increase in aircraft price based on the increase in operating empty mass. Both the mass of the LH2 tank and the fuselage structure increase due to the greater energy requirements at lower Mach numbers and altitudes, whereas the other designs for the other fuels only require an increase in wing area to accommodate the fuel.

4.6 Exemplary scenario for different fuel prices

The following diagram (Figure 15) shows the relative change in cost over the long-term climate impact (ATR100) of the various Jet-A1, SAF and LH2 designs, relative to the values of the Jet-A1-fueled baseline configuration with a fuel cost for Jet-A1 of 15 €/GJ. Four cost scenarios (15 €/GJ, 30 €/GJ, 45 €/GJ, 60 €/GJ) are considered for each fuel type and demonstrate the impact of increasing fuel costs. For a given price scenario of Jet-A1, SAF and LH2, these generic cost assumptions can be utilized for interpolation.

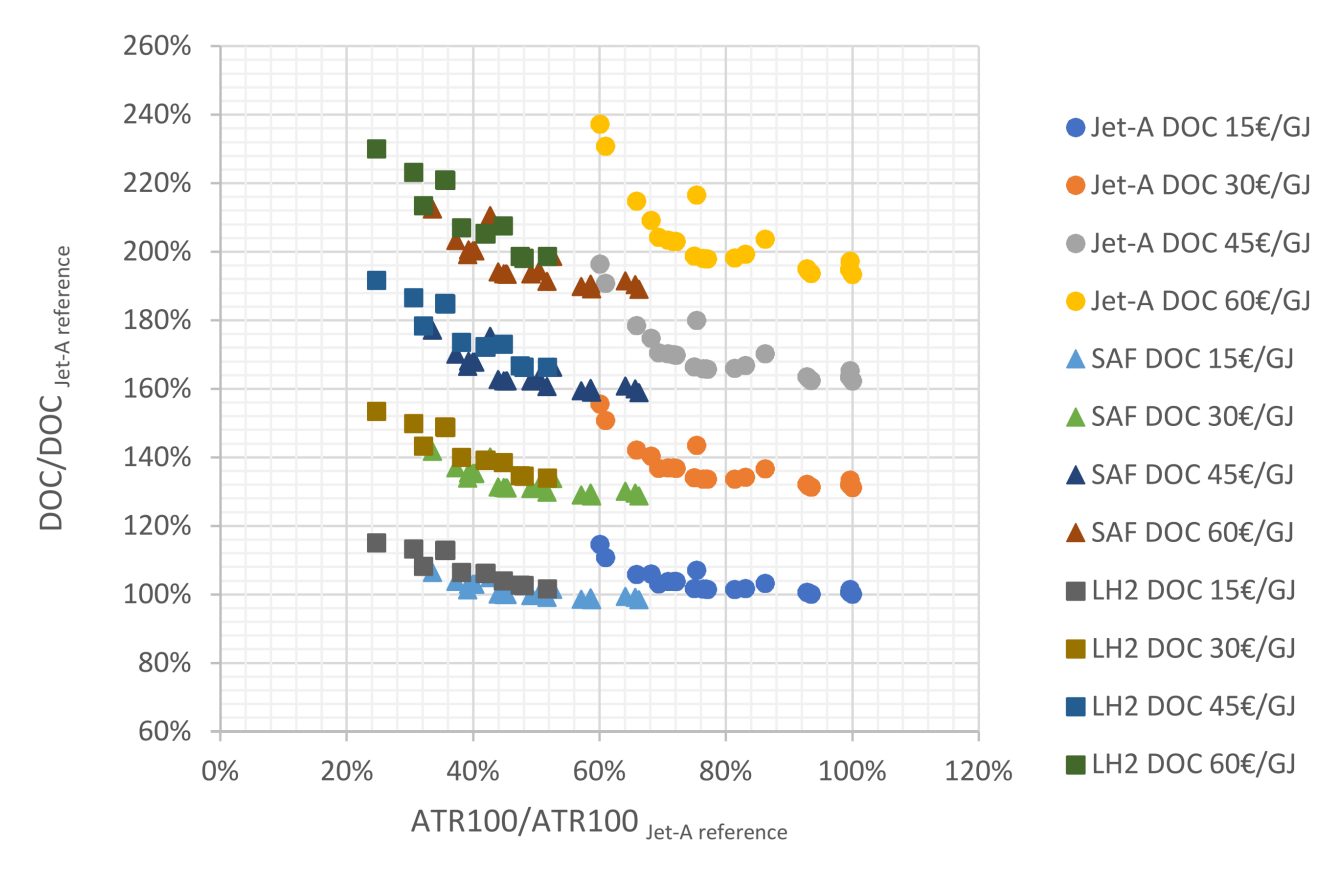


Figure 15 – Summary of the results of all kerosene, SAF, and LH2 configurations for different energy costs scenarios (15 €/GJ - 60 €/GJ). The relative changes of DOC and ATR100 are related to the Jet-A1 baseline (Mach 0.85, flight altitude limit 43 kft, 15 €/GJ)

The utilization of fossil kerosene along with lower altitude limits and reduced flight Mach numbers offer a reduction in ATR100 by about 40%. The use of SAF without any modifications of the design Mach number and altitude constraints reduces the ATR100 by around 35% compared to kerosene. In this case it is assumed that the influence of CO2 is 100% eliminated by SAF, which reduces the total impact by 23%. In addition, the impact of CiC is reduced due the reduced particulate emissions. Under the same conditions, LH2 offers an additional improvement of ca. 15% compared to SAF. Under consideration of the altitude constraints and adapted flight Mach numbers, the SAF configurations offer a reduction in ATR100 of around 66% compared to the kerosene baseline or about 30% when compared to the most radical kerosene configuration. The utilization of LH2 provides additional 10% reduction in ATR100 compared to the SAF configuration with the lowest climate impact. The cost impact depends on the scenario. A doubling of energy costs tends to increase DOC by about 30%. The increase in DOC for the reduced Mach number and altitude limitation is due to the increased fuel consumption and longer block times when flying slower and therefore fewer flights can be performed annually.

5. Conclusion

The study highlights the climate and direct operating cost impacts of fossil kerosene, SAF and LH2 on a derived long-range market scenario in 2035. In order to identify a suitable reference aircraft and a representative route network to be evaluated, a market analysis for the long-range market segment in 2019 is presented. The methodology applied is then described in detail and the baseline aircraft designs, comparable to today's flight characteristics in terms of cruise Mach number and flight altitude, are evaluated for each energy carrier option. Finally, a variation of flight Mach number and altitude restriction is demonstrated to further improve the climate impact of aviation at increasing cost. The results of this study for the two separate application cases are summarized:

When maintaining maximum flight altitude and Mach number:

- Switching from Jet-A1 to SAF could reduce the climate impact by around 35%. As has already been demonstrated in practice, existing aircraft can be used with minor modifications.
- In terms of aircraft design for the next generation of aircraft only minor modifications have to be made with respect to the different SAF characteristics (especially density and lower heating value).
- A transition to liquid hydrogen would reduce the climate impact by 50%. However, the related aircraft, engines, and systems would need to be completely redesigned, and would introduce a high degree of uncertainty.
- With respect to the DOC, the viability of the different energy carriers is highly dependent on future fuel prices, as the other cost factors are expected to be similar for the long range application.

When reducing the maximum flight altitude and adjusting of the cruise Mach number:

- By limiting the maximum flight altitude, further climate impact potential can be realized with increasing DOC. This will require a redesign of the aircraft, as optimum flight trajectories, wing planform and engine design will need to be adjusted accordingly.
- Switching from Jet-A1 to SAF can reduce climate impact by up to 66%, while increasing operating costs by at least 15%, depending on fuel prices.
- With the introduction of hydrogen, the climate impact could be further reduced by up to 75%. This is the maximum potential identified in this study and therefore climate neutral aviation cannot be achieved even with hydrogen.
- With SAF and hydrogen, there is no clear answer to the question of costs. The available scenarios cover a wide range and are naturally subject to major uncertainties.

Hence, the economics of SAF and hydrogen as fuel options for the long range market are highly dependent on the fuel price. Therefore, a generic cost scenario was derived to assist in the decision making process and to interpolate the DOC for a specific price scenario that was beyond the scope of this study. In addition, the uncertainties associated with hydrogen as an energy source in terms of aircraft design, engine design and emissions, and climate impact are more severe compared to the use of SAF. The latter has already been flight tested regarding the impact on aircraft application and climate.

Further studies and testing have to be conducted to allow for a more profound assessment of the hydrogen aircraft and engines. Specific fields of research related to manufacturing, maintainability and operability of the aircraft as well as emissions of hydrogen combustion and the climate impact of hydrogen are part of the European research program Clean Aviation, the German funded LuFo program and internal DLR projects, where findings of this study will be addressed.

6. Contact Author Email Address

Sebastian Wöhler,

German Aerospace Center (DLR),

Institute of System Architectures in Aeronautics, Hamburg, Germany

mailto: sebastian.woehler@dlr.de

7. Copyright Statement

The authors confirm that they, and/or their company or organization, hold copyright on all of the original material included in this paper. The authors also confirm that they have obtained permission, from the copyright holder of any third-party material included in this paper, to publish it as part of their paper. The authors confirm that they give permission, or have obtained permission from the copyright holder of this paper, for the publication and distribution of this paper as part of the ICAS proceedings or as individual off-prints from the proceedings.

References

- [1] German Aerospace Center, "TOWARDS ZERO-EMISSION AVIATION How DLR's Aviation Research Strategy supports the European Green Deal 2050," booklet, DLR, Cologne, Germany, 2021.
- [2] V. Williams, R. Noland, and R. Toumi, "Reducing the climate change impacts of aviation by restricting cruise altitudes," *Transportation Research Part D: Transport and Environment*, vol. 7, no. 6, pp. 451–464, 2002.
- [3] C. Frömming, M. Ponater, K. Dahlmann, V. Grewe, D. Lee, and R. Sausen, "Aviation-induced radiative forcing and surface temperature change in dependency of the emission altitude," *Journal of Geophysical Research D: Atmospheres*, vol. 117, no. 19, 2012.
- [4] K. Dahlmann, A. Koch, F. Linke, B. Lührs, V. Grewe, T. Otten, D. Seider, V. Gollnick, and U. Schumann, "Climate-compatible air transport system—climate impact mitigation potential for actual and future aircraft," *Aerospace*, vol. 3, no. 4, 2016.
- [5] Sabre AirVision Market Intelligence, "Data Based on Market Information Data Tapes (MIDT)," databank, Sabre, https://www.sabre.com/products/market-intelligence/, 2021. accessed on 24.2.2021.
- [6] International Civil Aviation Organization, "Civil Aviation Statistics of the World and ICAO staff estimates," annual report, ICAO, Montreal, Canada, 2019.
- [7] Graver, B., Rutherford, D., Zheng, S., "CO2 Emissions From Commercial Aviation: 2013, 2018, and 2019," booklet, International Council on Clean Transportation, https://theicct.org, 2020.
- [8] International Air Transport Association, "IATA Annual Review, 2021," annual review, IATA, Montreal, Canada, 2021.
- [9] Airbus S.A.S., "A350 aircraft characteristics airport and maintenance planning," manual, Airbus, 31707 Blagnac Cedex, France, 2017. June 2019.
- [10] Boeing Commercial Aircraft, "787 airplane characteristics for airport planning," technical report, Boeing, 2018. March 2018.
- [11] S. Wöhler, T. Burschyk, J. Häßy, and M. Iwanizki, "Design and assessment of long-range aircraft concepts with focus on fossil kerosene, sustainable aviation fuel and liquid hydrogen as energy carriers," in *AIAA AVIATION Forum 2023*, (San Diego, USA), American Institute of Aeronautics and Astronautics, 2023.
- [12] S. Wöhler, G. Atanasov, D. Silberhorn, B. Fröhler, and T. Zill, "Preliminary aircraft design within a multidisciplinary and multifidelity design environment," in *Aerospace Europe Conference 2020*, (Bordeaux, France), 2020.
- [13] B. Boden, J. Flink, N. Först, R. Mischke, K. Schaffert, A. Weinert, A. Wohlan, and A. Schreiber, "Rce: An integration environment for engineering and science," *SoftwareX*, vol. 15, p. 100759, 2021.
- [14] T. Burschyk, Y. Cabac, D. Silberhorn, B. Boden, and B. Nagel, "Liquid hydrogen storage design trades for a short-range aircraft concept," in *German Aerospace Congress (DLRK)*, *Bremen*, 2021.
- [15] P. Madden and K. Park, "Methodology for predicting nox emissions at altitude conditions from ground level engine emissions and performance test information."
- [16] P. Wehrel, R. Schöffler, C. Grunwitz, F. Carvalho, M. Plohr, J. Häßy, and A. Petersen, "Performance and Emissions Benefits of Cooled Ceramic Matrix Composite Vanes for High-Pressure Turbines," *Journal of Engineering for Gas Turbines and Power*, vol. 145, p. 121016, 10 2023.
- [17] A. Döpelheuer, Anwendungsorientierte Verfahren zur Bestimmung von CO, HC und Ruß aus Luftfahrttriebwerken. Dissertation, Ruhr-Universität Bochum, Bochum, 2002.

- [18] D. Ahrens, Y. Méry, A. Guénard, and R. C. Miake-Lye, "A New Approach to Estimate Particulate Matter Emissions From Ground Certification Data: The nvPM Mission Emissions Estimation Methodology," *Journal of Engineering for Gas Turbines and Power*, vol. 145, p. 031019, 12 2022.
- [19] F. Linke, Ökologische Analyse operationeller Lufttransportkonzepte. PhD thesis, Dt. Zentrum für Luft-und Raumfahrt, Bibliotheks-und Informationswesen, 2016.
- [20] F. Linke, "Trajectory Calculation Module (Teil I: VNAV)—Entwicklung Eines Simulink-Moduls zur Vorhersage Realer Flugzeugtrajektorien," Internal Report IB 328-2008-01, Deutsches Zentrum für Luft- und Raumfahrt, Hamburg, Germany, 2008.
- [21] V. Grewe and A. Stenke, "Airclim: an efficient climate impact assessment tool," *Atmospheric Chemistry and Physics*, vol. 8, p. 4621–4639, 2008.
- [22] K. Dahlmann, A. Koch, F. Linke, B. Lührs, V. Grewe, T. Otten, D. Seider, V. Gollnick, and U. Schumann, "Climate-compatible air transport system—climate impact mitigation potential for actual and future aircraft," *Aerospace*, vol. 38, 2016.
- [23] A. Stenke, V. Grewe, and M. Ponater, "Lagranian transport of water vapor and cloud water in the echam4 gcm and its impact on the cold bias," *Climate Dynamics*, vol. 31, p. 491–506, 2008.
- [24] U. Burkhardt and B. Kärcher, "Process-based simulation of contrail cirrus in a global climate model," *Journal of Geophysical Research*, vol. 114, 2009.
- [25] D. Silberhorn, K. Dahlmann, A. Görtz, F. Linke, J. Zanger, B. Rauch, T. Methling, C. Janzer, and J. Hartmann, "Climate impact reduction potentials of synthetic kerosene and green hydrogen powered mid-range aircraft concepts," *Applied Sciences*, vol. 12, no. 12, 2022.
- [26] J. Thorbeck, "From aircraft performance to aircraft assessment," dglr-bericht, DGLR, Bonn, Germany, 2007.
- [27] M. Beltramo, D. Trapp, B. Kimoto, and D. Marsh, "Parametric Study of Transport Aircraft Systems Cost and Weight," contractor report, NASA, Los Angeles, USA, 1977.
- [28] J. Hoelzen, D. Silberhorn, T. Zill, B. Bensmann, and R. Hanke-Rauschenbach, "Hydrogen-powered aviation and its reliance on green hydrogen infrastructure—review and research gaps," *Int. J. Hydrogen Energy* 2021, vol. 47, 2021.
- [29] D. Silberhorn, J. Hartmann, N. Dzikus, G. Atanasov, T. Zill, J. Gomez Trillos, M. Oswald, U. Brand, T. Vogt, and W. Grimme, "The air-vehicle as a complex system of air transport energy systems," in AIAA AVIATION Forum 2020, (Virtual Event), American Institute of Aeronautics and Astronautics, 2020.
- [30] U. E. I. Administration, "Annual Energy Outlook 2023," annual report, USEIA, https://www.eia.gov/outlooks/aeo/, 2023.
- [31] BP, "Approximate conversion factors statistical review of world energy," technical report, BP, 2021. updated July 2021.
- [32] Boeing Commercial Aircraft, "777-200lr/-300er/-freighter airplane characteristics for airport planning," technical report, Boeing, 2015. May 2015.
- [33] Airbus S.A.S., "A380 aircraft characteristics airport and maintenance planning," manual, Airbus, 31707 Blagnac Cedex, France, 2016. Dec 2016.
- [34] Airbus S.A.S., "A330 aircraft characteristics airport and maintenance planning," manual, Airbus, 31707 Blagnac Cedex, France, 2017. Jan 2017.

Appendix

Table 5 – The ranking of the first 5 routes in the long-haul segment (> 4000 km) with the most operations (flights)

Rank	Airport 1	Airport 2	Flights
1	JFK	SFO	15241
2	JFK	LHR	14072
3	HNL	LAX	11932
4	EWR	SFO	11611
5	BOS	LAX	10422

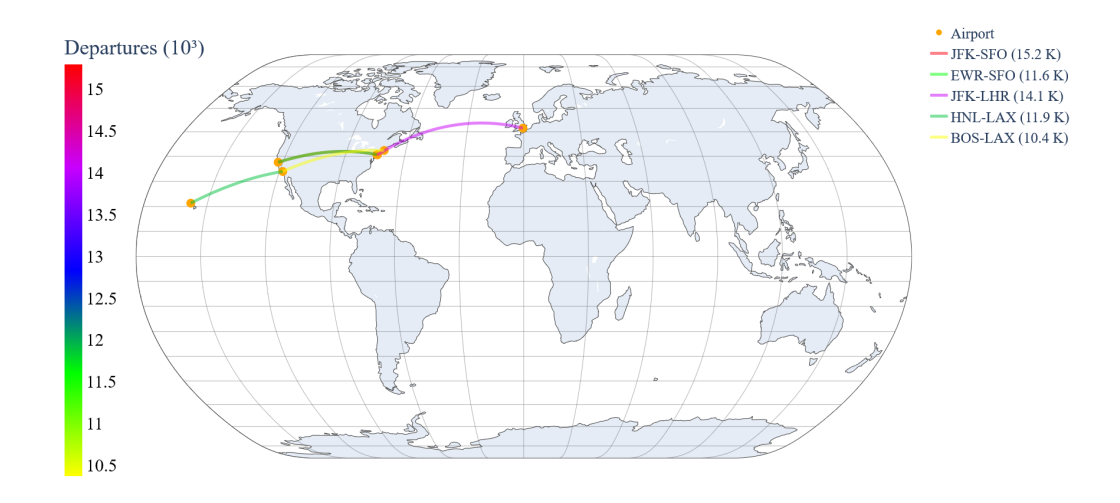


Figure 16 – The 5-best performing long-haul routes in the world (> 4000 km) in 2019 with the most operations (flights)

Table 6 – The world's top 5 busiest long-haul routes (> 4000 km) in 2019 with the highest passenger traffic

Rank	Airport 1	Airport 2	Distance	Pax
			[km]	[Mio]
1	JFK	LHR	5560	2.972
2	HNL	LAX	5527	2.362
3	DXB	LHR	4116	2.270
4	JFK	SFO	4160	1.998
5	EWR	SFO	4129	1.971

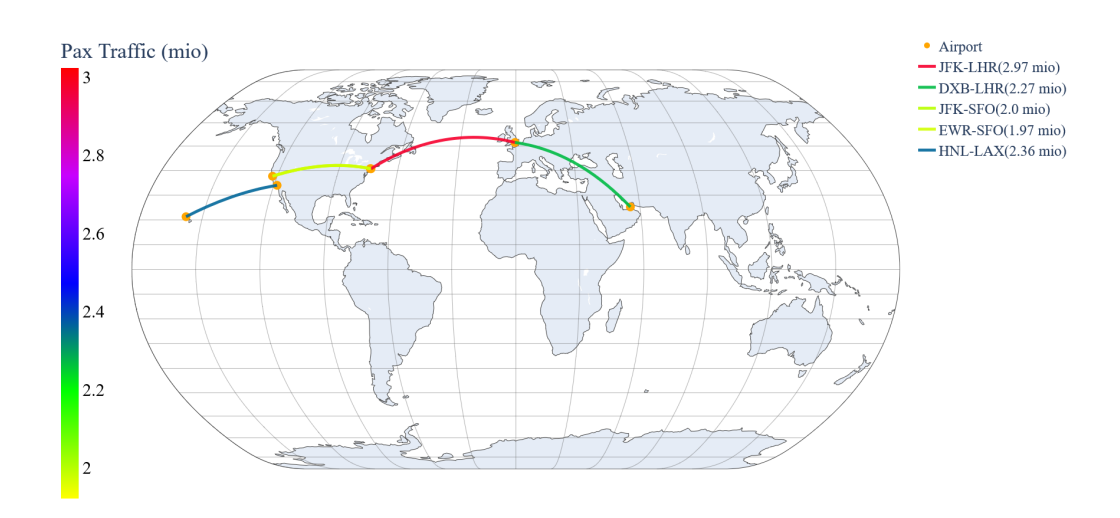


Figure 17 – The world's busiest long-haul flight routes (> 4000 km) in 2019 with the highest passenger traffic

Climate Impact and Economic Assessment of LH2 and SAF Long-Range Aircraft Concepts

Table 7 – The top 5 long-haul routes in the world with the most ASKs (Available Seat Kilometers) and RPKs (Revenue Passenger Kilometers)

Rank	Airport 1	Airport 2	Distance [km]	ASK [Mio]	RPK [Mio]
1	JFK	LHR	5536	21.230	16.467
2	SIN	LHR	10875	21.067	18.271
_	SIIV	LIIII	10073	21.007	10.271
3	HKG	LHR	9661	17.854	15.245
4	LAX	LHR	8782	16.332	13.315
7		LIIII	0702	10.552	10.010
5	DXB	LHR	5527	15.055	12.481

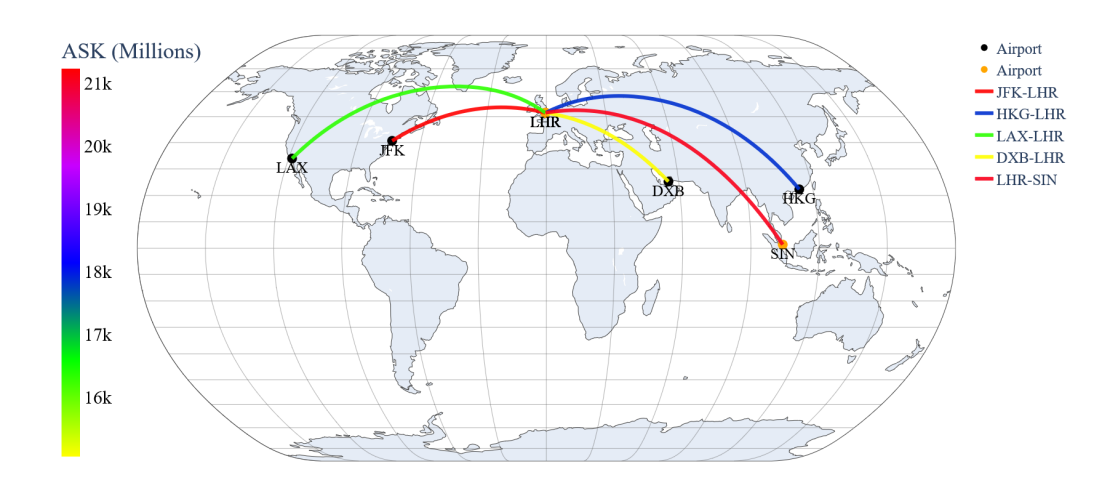


Figure 18 – The 5-best performing long-haul routes in the world (> 4000 km) in 2019 with the most ASKs

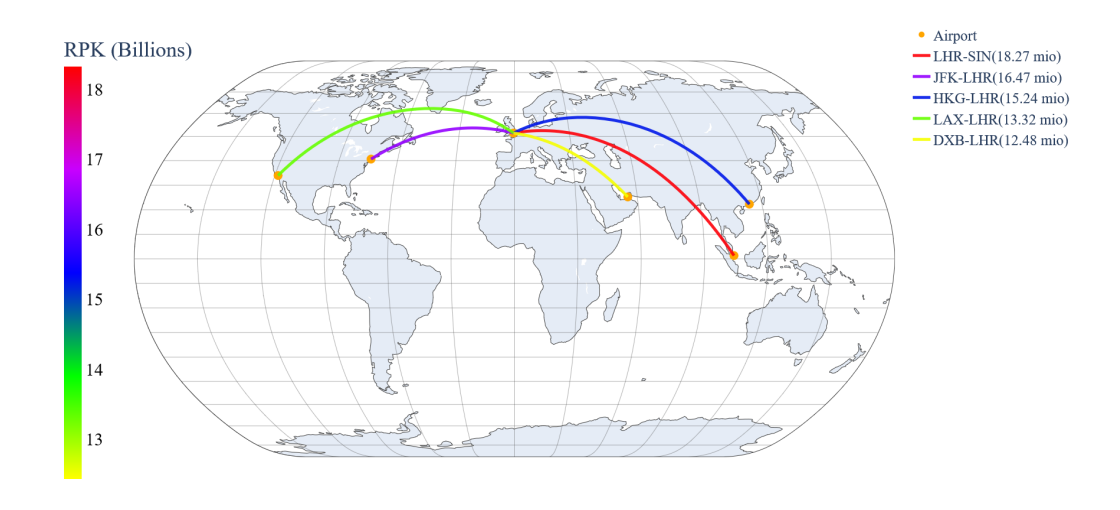


Figure 19 – The 5-best performing long-haul routes in the world (> 4000 km) in 2019 with the most RPKs

Climate Impact and Economic Assessment of LH2 and SAF Long-Range Aircraft Concepts

Table 8 – The ranking of the top 5 long-haul routes with the highest CO2 emission density per km flown in 2019

Rank	Airport 1	Airport 2	Distance [km]	CO2 Emission Density [ton/km]
1	JFK	LHR	5560	392.2
2	DXB	LHR	5527	262.6
3	SIN	LHR	10916	212.9
4	SIN	SYD	6337	212.5
5	SIN	MEL	6078	196.4

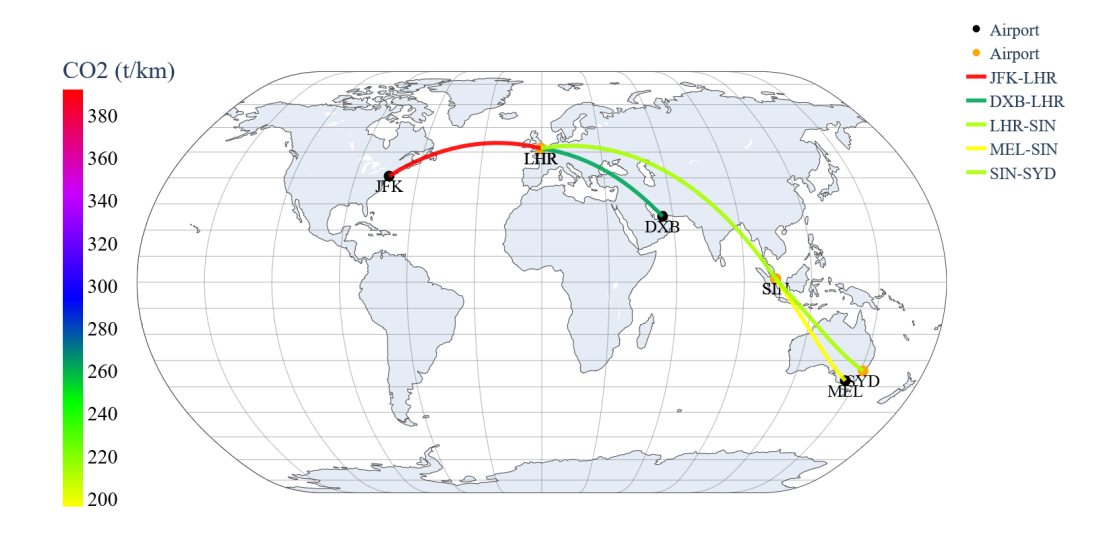


Figure 20 – The ranking of the long-haul routes with the highest CO2 emission density per km flown in the world (> 4000 km) in 2019

Table 9 – The ranking of the top 5 aircraft types with the most seat kilometers flown and their average seat capacity on long-haul routes (> 4000 km) in 2019

Rank	IATA Code	ICAO Code	Aircraft type [ref]	Operating Airline ASK [Mio]	Operating Airline ASK [%]	Average number of seats	Typical number of seats
1	77W	B773	Boeing 777-300ER[32]	746.252	18.9	347	365
2	789	B789	Boeing 787-9 [10]	410.987	10.4	280	290
3	388	A388	Airbus A380-800 [33]	384.865	9.7	499	575
4	333	A333	Airbus A330-300 [34]	332.794	8.4	290	300
5	359	A359	Airbus A350-900 [9]	253.729	6.4	298	315